Selection and Characterization of Semi-Automated Disinfection Devices: Findings and Recommendations from Boeing Research & Technology

Katherine Lastoskie, Sabyasachi Basu, Mark Wilson, Sandra Martinez-Compton, Arzan Dotivala, Steven Domagalski, and Neil Shah
Corresponding Author: Neil Shah

Executive Summary

In the wake of the global COVID-19 crisis, thorough and efficient cleaning procedures are desired to support a healthy environment and cost-effective return to pre-pandemic air traffic levels. This paper presents initial research findings on semi-automated disinfection methods, which can provide the ability to disinfect surfaces more consistently and efficiently than manual application of chemicals.

Boeing conducted two studies, called Design of Experiment (DOE) 1: Characterization of Electrostatic Sprayer Application of Disinfectants and DOE 2: Wetting and Drying of Representative Substrates, to characterize electrostatic spray disinfection devices (one type of semi-automated device). Based on those studies and as discussed in greater detail below, the following is recommended with respect to electrostatic spray devices:

- Do not use fogger type semi-automated disinfection, based on potential risks to environmental control system components.
- When using an electrostatic spray device:
  - Use a device that generates a cone shaped spray pattern.
  - Maintain a distance of 2-4 feet between the nozzle and surface.
  - Move the nozzle of the sprayer through a 90 degree arc in roughly 5 seconds to establish a baseline spray traverse speed.
  - Note that within a 40-80% humidity and 68-90.5°F range, the required dry time of non-porous materials increases inversely with temperature, proportionally to the percentage relative humidity.

Further evaluation of safety-critical flight hardware is necessary prior to recommending models of electrostatic spray devices and specific disinfectants for general use. This paper does not address the compatibility of the studied disinfectants with aircraft materials. Aircraft carriers should consult the most recent Multi Operator Message (MOM) from Boeing to ensure appropriate disinfectant selection

Introduction

Addressing New Challenges in the Commercial Aviation Industry

An outcome of the COVID-19 pandemic is an increased need for healthy, disinfected public spaces. It is imperative to reduce risk in the commercial aviation industry, which moved 1 billion people across the globe in 2019.[1] Widespread public concerns of the health risks of travel have not subsided, despite data that suggest that engineering controls such as high volume air recirculation and filtration substantially reduce the risk of disease transmission in flight.[2,3] Aircraft passengers will also continue to expect reasonable gate turnaround times, and competitive aircraft fares, even as more rigorous disinfection is performed between flights.

Thorough and efficient cleaning procedures must be implemented to return to pre-pandemic air traffic levels quickly and cost-effectively. For air carriers to retain an average turn-around time of

30 minutes for a single aisle aircraft, the target disinfection duration is 10 minutes. Manual application of disinfectant, with spray bottles and cleaning cloths, cannot be completed in the targeted timeframe without a significant increase in the cleaning crew manpower and therefore cost. Another challenge is the possible variability of manual cleaning. Evenness of application on contaminated surfaces is important, but cannot be guaranteed between individuals who may spray with different timing, frequency and force. This underscores the important potential of using semi-automated mechanisms for disinfectant application.

Semi-Automated Disinfection Device Considerations

Semi-automated disinfection devices aerosolize a liquid disinfectant into a spray of small particles (0.5-120 microns [µm] in size). A crew person in personal protective equipment (PPE) would use the device to apply a layer of aerosolized disinfectant to surfaces in the aircraft. This will vary between different individuals' application techniques, but is more likely even and uniform compared to manual application. These devices are commercially available and use a variety of technology types to aerosolize and distribute droplets.

Boeing evaluated three types of semi-automated disinfection devices: Electrostatic Sprayer (ES) devices, Ultra-Low Volume (ULV) Foggers, and Cold Plasma Foggers. Of the three, ES devices were selected for further characterization due to the ease of operational use, and the probability that the comparably larger droplet size would be a smaller risk for intake into the aircraft's environmental control system components. For additional information refer to Appendix 8.1.

Chemical Disinfectant Considerations

Simultaneous to the selection of the ES device type, an evaluation of possible disinfectant candidates was conducted. Disinfectants were down selected from the United States Environmental Protection Agency (EPA) List N: Disinfectants for Use Against SARS-CoV-2 (COVID-19) in March of 2020. The criteria included demonstrated efficacy at inactivation of SARS-CoV-2, demonstrated efficacy against pathogens that are more difficult to inactivate than SARS-CoV-2, or demonstrated efficacy against a human coronavirus similar to SARS-CoV-2. Further, airplane safety concerns eliminated certain disinfectants from List N and are detailed in Appendix 8.2. The selected disinfectants were: Calla and Matrix #3 (quaternary ammonium compounds), Peroxi™ RTU (life science laboratory formulation of an Accelerated Hydrogen Peroxide®), and PREempt™ RTU (aerospace and hospital formulation of an Accelerated Hydrogen Peroxide®).

2.4 Boeing Research Objectives

Research conducted at Boeing and the University of Minnesota was used to select commercially available ES device models and characterize the droplet distribution shape, droplet size, and mean electrostatic charge of each device. The full reports are in Appendix 8.3 and Appendix 8.4 respectively.

From this initial work, the following models were selected: the EvaClean™ Protexus PX300ES Cordless Electrostatic Backpack Sprayer, the EMist EM360 Cordless Electrostatic Backpack Sprayer and the Electrostatic Spraying Systems (ESS) SC-MB Corded Suitcase-Style Sprayer. The DOE 1 and DOE 2 studies were then designed to evaluate the outcomes of using ES devices with deliberately varied operational parameters and conditions.

Methodology

3.1 DOE 1: Characterization of ES Devices from Varied Input Parameters

A test matrix was created using principles of statistical Design of Experiments (DOE) to vary input parameters (Table 1). The deposition were measured by weight gain and dry time. By systematically controlling the variables, 695 tests were used to build a statistical model to predict the outputs of all possible combinations. For more information, refer to Appendix 8.5.

In each test, a 3-by 4-foot material coupon was sprayed by a person. The ES device was swept through a 90-degree arc in 5 or 10 seconds; an approximation of the speed at which a crew person might disinfect a space.

Table 1: The variable input parameters of the DOE 1 study

Parameter	Factors
Sprayer	EvaClean™ Protexus Sprayer (40 and 80 µm); ESS SC-MB Sprayer; EMist EM360 Sprayer (85 µm)
Disinfectant Solutions	Calla® ; Peroxi™ RTU; PREempt™; Matrix #3
Surface Materials	Porous (40lb Kraft Paper); Non-porous (Polycarbonate)
Spray Time	5 seconds; 10 seconds
Spraying Distance from Object	2 feet; 4 feet; 6 feet
Fan Circulation	Circulation, No Circulation
Orientation of the Surface Material and Spray Direction	Sample on ground: sprayed perpendicular, and down at 45°; Sample on wall: sprayed perpendicular, up and down at 45°; Sample at 45°: sprayed perpendicular, up and down at 45°

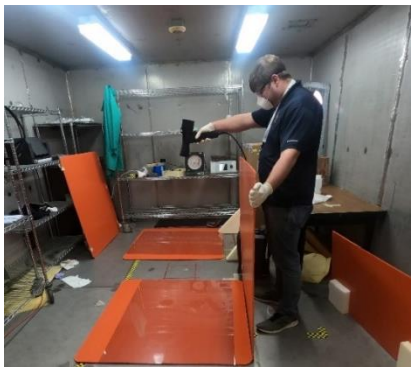

Figure 1: A handheld electrostatic sprayer held perpendicular to a sample on the ground.

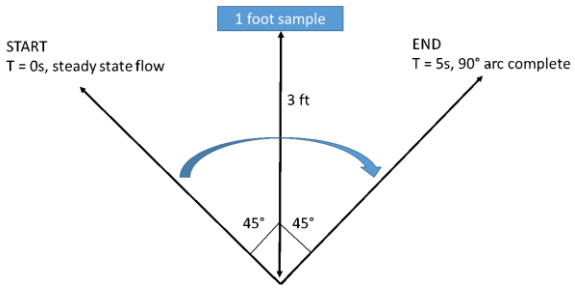

Figure 2: The spray pattern established for the DOE studies

3.2 DOE 2: Deposition and Drying of Material Substrates at Varied Input Parameters

The DOE 2 study also leveraged statistical DOE principles to evaluate the deposition and drying impacts of variable input parameters (Table 2). Various materials representative of those found in an aircraft were also used (Table 3).

In each test, a tester used an electrostatic sprayer to deposit disinfectant on a 1-by 1-foot material coupon. The outputs were quantified using a FLIR® E40 Thermal Imaging Camera. The camera was mounted to a tripod for stable data collection and used to record a 15 minute video for each line item in the test matrix.

The settings on the camera were manually adjusted so that a fixed temperature range could be used. To eliminate noise, the data collector left the site immediately after spray application during the recording. This reduced airflow and vibration effects.

Temperature changes, captured with pixel density analysis, were used to measure deposition and drying time. Automated processing was used to remove subjective interpretation of deposition and drying time, and a mathematical model was fit to the IR data. In some cases, unexpected sources of noise prevented this method from being applied. Manual estimates were used, or the affected videos were excluded. The full methods are provided in Appendix 8.6.

Table 2: The variable input parameters of the DOE 2 study

Parameter	Factors
Temperature	Ambient 70°F; High, 85°F
Humidity	Ambient, 40% RH; High, 80% RH
Surface	Curved (Figure 8C) Porous Materials Only*; Flat
Replications	1 per condition; 2 per condition
Orientation and Spray Angle	Material on Wall – Perpendicular Spray; Material on Ground – Perpendicular Spray; Material on Ground – 45° Spray

Table 3: The materials used in the DOE 2 study

Non-porous/Porous	Category	Material Type	Specification
Porous	Rubber	Silicone	BMS 1-72
Porous	Curtain	Polyester	BMS 8-240 Cl 1 Gr D Ty I/IV
Porous	Carpet	Wool/Nylon Blend	BMS 8-237 TY II CL 1 Gr A Comp C
Porous	Carpet	Wool	BMS 8-237 Comp A
Non-porous	Metal	Al 2024-T3 Clad	QQ-A-250/5, AMS 4041
Non-porous	Metal	Al 2024-T3 Bare	QQ-A-250/4, AMS 4037
Non-porous	Metal	Al 7075-T6 Bare	QQ-A-250/12, AMS 4045
Non-porous	Paint	Flight Deck Coating	BMS 10-83 Ty III
Non-porous	Paint	Cabin Coating	BMS 10-83 TY VII
Non-porous	Sidewall	PEKK	BMS 8-320
Non-porous	Window	Tedlar	(Window Shade Tedlar Film over PEKK)
Non-porous	Stowbin	PVF	BAC5596 Ty IVA
Non-porous	Window	PEI (Ultem)	Ultem 9085
Non-porous	Window	Polycarbonate	BMS 8-251 Ty III

Figure 3: A sample is stretched over a curved surface on the ground, and sprayed at 45^{o}

4 Results

Analysis of variance (ANOVA) was performed on the data from the DOE 1 and DOE 2 studies. A subset of this analysis is presented in the tables below to show statistically significant first level factors. In general, variations in factors that have a p-value under 0.05 will impact the deposition or dry time. The following main effects plots show these impacts and the overall effect of each input factor after average across all other factors. Note that the interaction of different factors could result in different outcomes than the sum of the main effects.

4.1 DOE 1 Results

4.1.1 Significant Factors on Dry Time

Dry time was statistically impacted by distance, fan setting, and the disinfectant used.

Table 4: Impact of input parameters on dry time

Factor	p-Value	Impact to Dry Time
Spray Distance	0.000	Significant
Fan	0.000	Significant
Disinfectant	0.004	Significant
Material	0.587	Not Significant
Material Orientation	0.616	Not Significant
ES Device	0.65	Not Significant

Figure 4 plots the impact of variable spray distance (between nozzle and sample) on material dry time. Dry time is inversely related to distance.

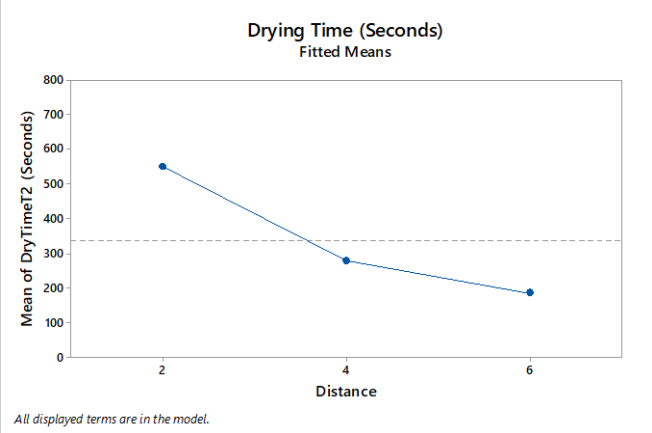

Figure 4: Dry time from varying distance

Figure 5 shows the impact of fan setting on material dry time. With no air circulation, the average dry time is approximately 250 seconds longer than average dry time with circulation.

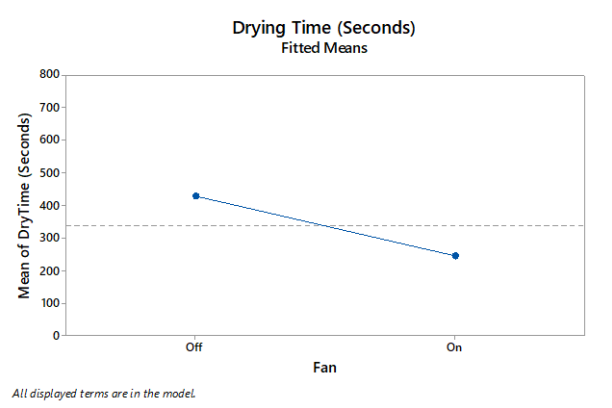

Figure 5: Dry time from varying circulation

Figure 6 indicates the impact of the particular disinfectant on dry time. Substrates sprayed with Matrix #3 and Preempt had longer dry times than those sprayed with Calla and Peroxi™ RTU.

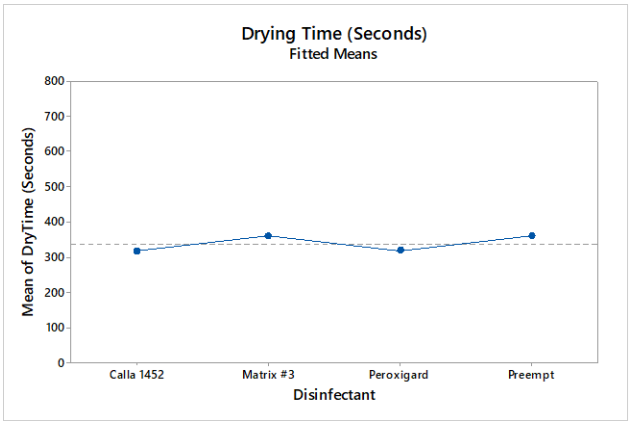

Figure 6: Dry time from varying disinfectant

4.1.2 Significant Factors on Weight Gain

Spray distance and ES device had a statistically significant impact on weight gain.

Table 5: Impact of input parameters on weight gain

Factor	p-Value	Impact to Weight Gain
Spray Distance	0.001	Significant
ES Device	0.004	Significant
Material	0.183	Not Significant
Material Orientation	0.435	Not Significant
Disinfectant	0.528	Not Significant
Fan	0.932	Not Significant

Figure 7 plots the impact of distance on weight gain. Weight gain is inversely proportional to distance.

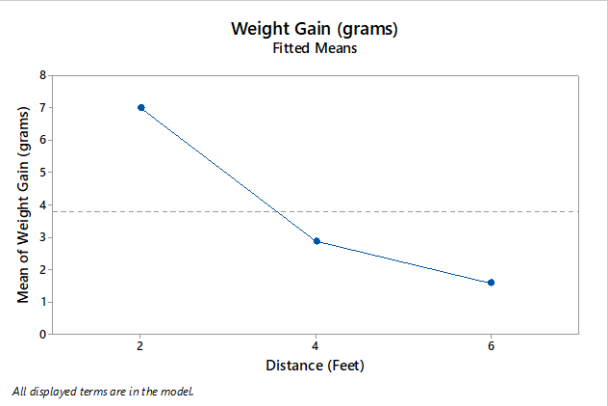

Figure 7: Weight gain from varying distance

Figure 8 shows weight gain by sprayer. The EMist EM 360 (85µm) sprayer deposited more disinfectant (5.5 g) than the EvaClean 80 µm, EvaClean 40 µm, and ESS 40 µm sprayers (3 g, 2.9 g, and 4.1 g respectively).

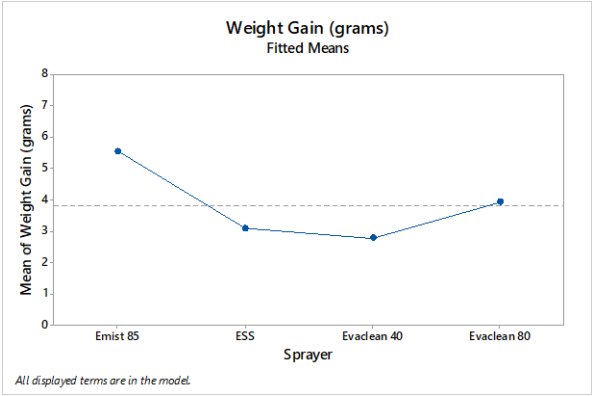

Figure 8: Weight gain from varying ES device

4.2 DOE 2 Results

4.2.1 Significant Factors on Dry Time

Orientation and geometry, and humidity had a statistically significant impact on dry time for both non-porous and porous materials. Material was an additionally significant factor for porous materials.

Table 6: ANOVA of drying times for porous materials

Factor	p-Value	Impact to Dry Time of Porous Materials
Orientation and Sprayer Geometry	<0.001	Significant
Humidity	<0.001	Significant
Material	0.003	Significant
Disinfectant	0.026	Borderline
Sprayer Flow Rate	0.109	Not Significant
Temperature	0.963	Not Significant

Table 7: ANOVA of drying times for non-porous materials

Factor	p-Value	Impact to Dry Time of Non-porous Materials
Orientation and Sprayer Geometry	<0.001	Significant
Humidity	0.001	Significant
Temperature	0.085	Borderline
Material	0.159	Not Significant
Disinfectant	0.167	Not Significant
Sprayer Flow Rate	0.585	Not Significant

Figure 9 and Figure 10 plot the dry time by varied orientation and ES position on porous and non-porous materials, respectively. The dry time is longer for coupons sprayed on the ground as compared to those on the wall. One explanation is that gravity alters the trajectory of enough particles such that a significant portion are pulled down before making contact with the sample. This suspected higher deposition could explain the observed higher dry time.

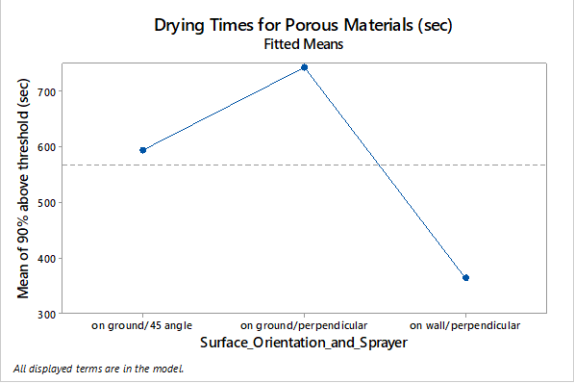

Figure 9: Drying time from varying orientation and sprayer geometry on porous materials

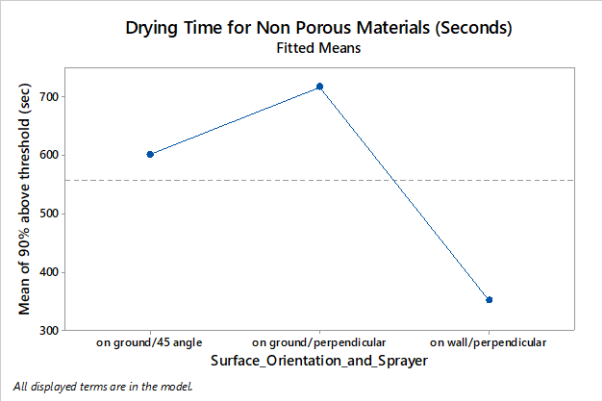

Figure 10: Drying time from varied orientation and sprayer geometry on non-porous materials

Figures 11 and 12 plot the impact of temperature and humidity on porous and non-porous materials, respectively. Dry time increases with humidity only for the porous materials.

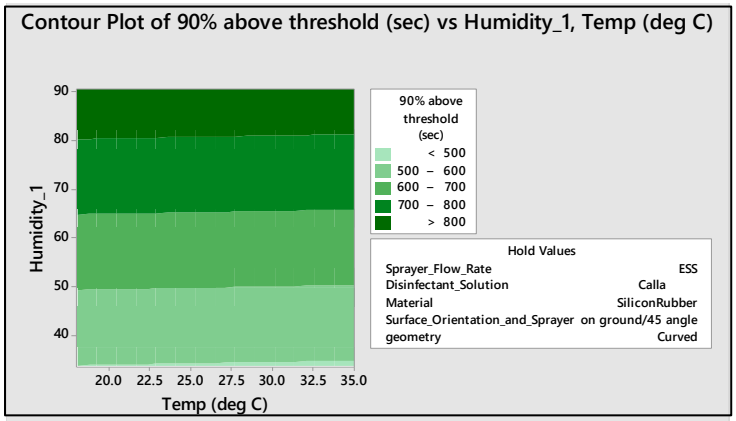

Figure 11: Contour plots of predicted drying time for porous materials

On the non-porous materials, both temperature and humidity influence the dry time. Ambient temperature and high humidity conditions generated the longest drying times. Conversely, high temperature and low humidity generated the shortest drying times.

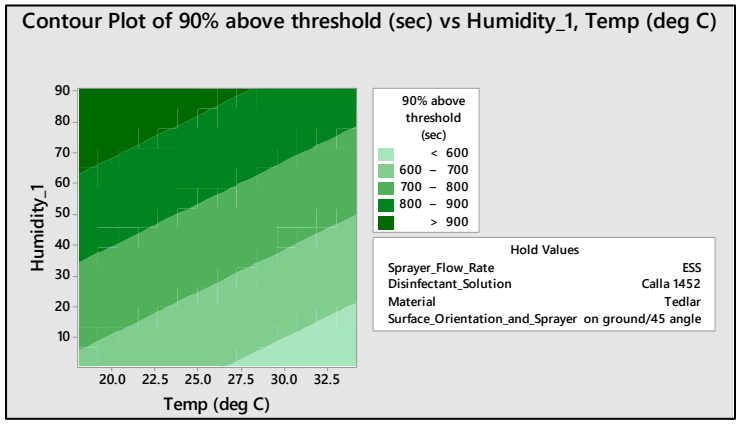

Figure 12: Contour plots of predicted drying time for non-porous materials

Figure 13 shows the dry time by porous material. For the porous materials, Silicone Rubber had the longest dry time and Wool had the shortest dry time.

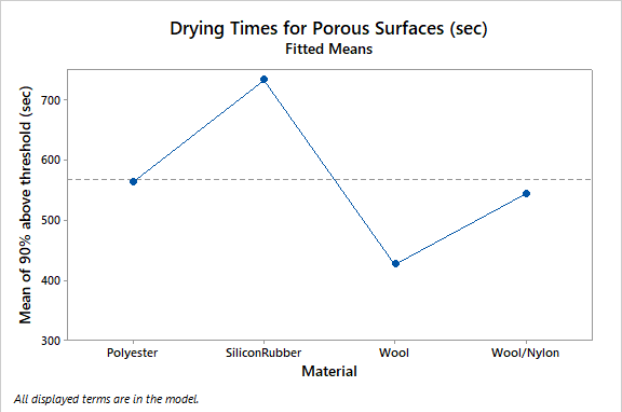

Figure 13: Drying times for different porous materials and orientations

5 Conclusions

Electrostatic sprayers have an advantage over conventional spray and wipe in that a large area can be covered with disinfectant in an efficient manner with minimal time. Importantly, spray droplets can attach to areas not directly in the sprayed path. No assessment of the effectiveness of periodic wiping after electrostatic spray application was conducted. However, periodic wiping of surfaces is recommended to remove surface contaminants and reduce the accumulation of surfactants.

Per the results in section 4, the following recommended best practices for the operation of ES devices were created for air carriers. Based on the potential risks that mists present to environmental control system components, Boeing does not recommend the use of fogger type semi-automated disinfection. Commercially available ES devices fitted with nozzles to create cone shaped spray patterns had equivalent performance related to deposition and dry time throughout the studies. The sprayer brand did control the positive or negative charge on the aerosolized liquid. The charge did not impact operational performance, but may contribute to the ability to destroy virus.

Boeing recommends spraying at distances between 2 and 4 feet. By keeping the spray distance under 4 feet, the operator can avoid insufficient deposition, especially if the spraying is upwards, or towards a vertical surface (Figure 7). As spray deposition amount is correlated to disinfection effectiveness, low deposition should be avoided. By keeping the distance at greater than 2 feet, the operator can control dry time. Spraying closer than 2 feet may result in significantly longer dry times (Figure 4).

When spraying non-porous materials, the DOE 2 results suggest that temperature and humidity had a definitive impact on dry time, particularly for non-porous materials. From contour plots presented in Figure 12, an ambient temperature (in the tested range of 68 to 90.5° Fahrenheit) and high humidity led to the longest dry times, *exceeding 15 minutes*.

Boeing also recommends that spraying be done using a sweeping motion, traversing a 90-degree arc in about 5 seconds. This appears to capture the natural human motion of spraying. We recognize that operators may not mimic the exact motion that was utilized in this study, and, in practice, a certain amount of learning will be required to create the appropriate motion to obtain the nominal amount of deposition.

Further evaluation of safety-critical flight hardware is necessary prior to recommending ES devices and specific disinfectants for general use. Appendix 8.7 details the continued research initiatives of Boeing Research & Technology on electrostatic spray technology. This paper does not address the compatibility of the studied disinfectants with aircraft materials. Aircraft carriers should consult the most recent Multi Operator Message (MOM) from Boeing to ensure appropriate disinfectant selection.

6. References

1. Air Traffic Organization, Affiliated Organizations. (2020). Air Traffic By The Numbers. Federal Aviation Administration.
2. Silcott, D., Kinahan, S., Santarpia, J., Silcott, B., Silcott, R., Silcott, P., . . . Accardi, R. (2020). Transcom/AMC Commercial Aircraft Cabin Aerosol Dispersion Tests. United States Transportation Command (USTRANSCOM) & Air Mobility Command (AMC).
3. T.H. Chan School of Publich Health, Harvard. (2020). Assessment of Risks of SARS-CoV-2 Transmission During Air Travel. Health, Harvard T.H. Chan School of Public. Cambridge: Unpublished.

7. Acknowledgements

The authors gratefully acknowledge the contributions of the following teammates:
Bradley Silva, Jay Covey, Bud Jewett, Michael Pearce, Ethan Moore, Mark Loeb, Lance Kephart, Alex Dunlap, James Hyink, Rovelyn Dytico, Angela Elting, Jill Seebergh, Kay Blohowiak, Bryan Moran, Shane Arthur, Nels Olson, and Stephen Jones

8. Appendix

8.1 Semi-Automated Device Considerations

An initial study by Boeing Research & Technology evaluated three types of commercially available, semi-automated disinfection devices: Electrostatic Sprayer (ES) devices, Ultra-Low Volume (ULV) Foggers, and Cold Plasma Foggers.

Table 1 summarizes the key considerations for each device type, including the Volume Median Diameter (VMD), electrostatic charge, and PPE required for operation. The VMD is the midpoint droplet size: one half of the volume is composed of droplets with diameters larger than the VMD, and one half is composed of droplets with diameters smaller than the VMD.

Table 1: Comparison of Semi-Automated Mechanisms

Property	ES Devices	ULV Foggers	Cold Plasma Foggers
VMD	20 to 120 μm	5 to 50 μm	0.5 to 9 μm
Electrostatic Charge	Unipolar Charge	Uncharged	Uncharged
Required PPE	Goggles, gloves, N95 respirator	Goggles, respirator, gloves, Tyvek suit	Goggles, Respirator, Gloves, Tyvek suit

ES devices work by spraying electrostatically charged droplets on a surface or an object. A water based disinfectant solution is combined with air and atomized by an electrode in the nozzle. ES devices are unipolar and apply a positive or negative charge to the droplets, depending on the particular device design. The small electrically charged droplets pass through

the nozzle and wrap around a surface. This creates a faster output and more uniform coverage than with manual application.

ULV foggers and cold plasma foggers also disperse antimicrobials into extremely small droplets with a VMD smaller than an ES device. However, this extremely small size could enable droplets to pass into return air ducts, posing a risk to environmental control system components, such as fan blades and filters. Foggers also require a higher level of personal protective equipment than ES devices. The SteraMist Surface Disinfection Unit, when dispersing a solution of 7.8% hydrogen peroxide, requires goggles, respirator, gloves, and a full Tyvek suit.

The cold plasma fogger evaluated was the TOMI™ SteraMist® Binary Ionization Technology® Surface Unit. It is a corded suitcase fogger for activation and ionization of a 7.8% solution of hydrogen peroxide into a fine mist or fog with a VMD of 0.5 to 9 µm containing reactive oxygen species including hydroxyl radicals for moderate to high level disinfection.

8.2 Chemical Disinfectant Considerations

Disinfectants considered for use were down selected from those on the United States Environmental Protection Agency (EPA) List N: *Disinfectants for Use Against SARS-CoV-2 (COVID-19)*. The disinfectants considered were:

1. Alcohols, including ethanol and isopropanol, which inactivate enveloped viruses by disrupting the lipid bilayer and denaturing its proteins.
2. Carbolic acids, such as phenols and thymol, which inactivate viral proteins and nucleic acids.
3. Reducers, such as l-lactic acid and citric acid, which inactivate virus by denaturation of viral proteins and disruption of the lipid bilayer.
4. Oxidizers, including chlorine dioxide, and peroxygens, such as hydrogen peroxide and peracetic acid, which inactivate virus by denaturation of proteins, disruption of the lipid bilayer, and oxidation of sulfur bonds in proteins.
5. Quaternary ammonium salts, such as benzylalkonium chloride, which inactivate virus by disruption of the lipid bilayer and denaturation of proteins.

The following criteria were applied to eliminate disinfectants:

a. Alcohols were eliminated because they are flammable. Small amounts can be used to wipe surfaces manually, but application with a charged semi-automated system could result in a hazardous condition.
b. Carbolic Acids, such as Phenols and Thymol, were eliminated due to health and safety concerns surrounding dermal absorption and potential allergic reactions.
c. Reducers, such as L-Lactic acid, were eliminated based on their potential to be corrosive. While reducers can be applied with electrostatic sprayers, they can be corrosive to airplane cabin materials depending on the concentration.
d. Certain Oxidizers were eliminated because they are highly corrosive depending on the concentration and contact time. Chlorines and Peracetic acid were ruled out especially at lower concentrations because they react to oxygen and water quickly after application.

8.3 ES Device Characterization: University of Minnesota Report

DROPLET ELECTROSTATIC CHARGE MEASUREMENT
TO SUPPORT COVID RESPONSE PROJECTS
Final Report

Qingfeng Cao, Seong Chan Kim, Qisheng Ou, Chenxing Pei, David YH Pui

Center for Filtration Research, Department of Mechanical Engineering, University of Minnesota
July 6, 2020

Project Introduction

The study is aimed to evaluate the mean charge level and droplet size distributions of two electrosprays from the Boeing Company, which are the Protexus model from EvaClean (Protexus) and the SC-EB model from ESS (SC-EB). The Protexus sprayer has three nozzle settings with the nominal droplet size being 40 μm, 80 μm and 110 μm, while the SC-EB sprayer has only one nozzle setting. Two disinfectant materials of the Calla and Peroxi solutions were applied for the tests. The Calla concentrated solution was diluted by the Type 1 DI water with a dilution rate of 4 oz of Calla solution in 1 gallon of DI water, and the Peroxi solution was tested without any dilution as instructed by Boeing. This report provides the mean droplet electrostatic charge and size distributions for all spray system and disinfectant combinations.

Droplets Size Distribution Measurement

The Global Sizing Velocimeter (GSV) system (TSI Model GSV-1000) was applied to characterize the droplet size generated by the two sprayers. It is a global imaging technique for simultaneous size and velocity measurement of transparent and spherical particles over a two-dimensional region. The size measurement is based on the angular oscillations of scattered light off a particle, which have uniform spacing inversely proportional to particle diameter. The velocity measurement is done by particle tracking analysis of two consecutive image frames with known time interval. For more background information on GSV technique, please refer to the published papers (Pan *et al*., 2005; Li and Massoli, 1994; Ragucci *et al*., 1990).

Figure 1 presents the schematic diagram of our GSV test stand, which is composed of a 532 nm double-pulsed laser, a high-resolution CCD camera installed at 60° scattering angle and a slit aperture placed in front of the camera lens to block all but a narrow string of the original out-of-focused image. The camera focuses at a plane slightly away from the light sheet (defocusing). Two parallel plates were installed at the measurement area with the plate distance to be 8 cm. Electric field was applied to the parallel plates by a voltage supply providing a voltage potential difference of 8 kV. The purpose of introducing the parallel plates is to generate a deflection velocity for each charged droplet in between. By knowing the deflection velocity and diameter, we can calculate the charge carried by the droplet. During each measurement, the distance between the sprayer nozzle and the measurement area was kept at about three feet. At this distance, good-quality images can be created for the GSV system to analyze.

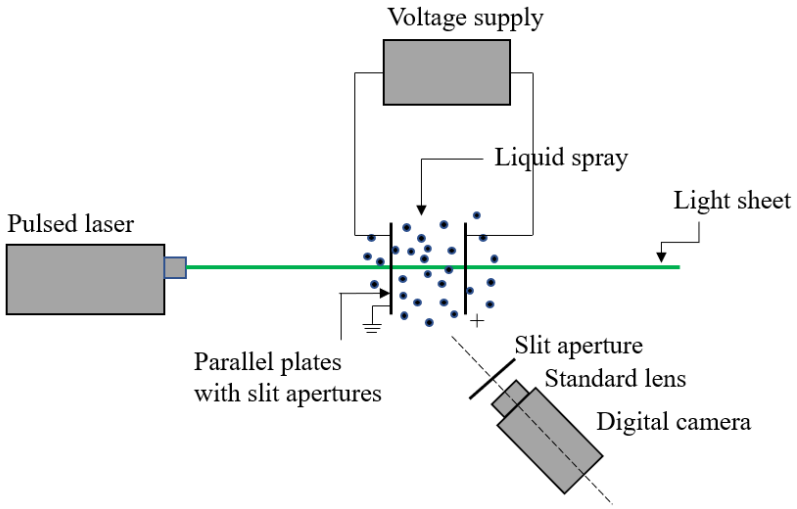

Figure 1. Schematic of the GSV system for measuring the droplet size and velocity.

Figure 2 and Figure 3 show the droplet size distributions generated by the Protexus sprayer with the Calla solution and Peroxi solution, respectively. All the three nozzle settings (40, 80, and 110 μm) have been tested. For each case, both the number and volume distributions were presented. From the number distributions, it can be observed that the sprayer generates more droplets smaller than 45 μm for all the nozzle settings. As we increased the nozzle setting from 40 μm to 110 μm, larger droplets were generated. For the 80-μm and 110-μm nozzle settings, size peaks at around 80 μm and 110 μm can be seen in the volume distributions, respectively, especially for the Calla solution.

Figure 4 indicates the droplet size distribution for the SC-EB sprayer with both the Calla and Peroxi solutions. The sprayer has only one nozzle, which generates smaller droplets than the Protexus sprayer with all the nozzle settings. This conclusion can also be made by comparing the measured mean droplet sizes presented in Table 1. Both the number mean diameter (NMD) and volume mean diameter (VMD) are included in the table. The Peroxi solution has slightly larger droplet size than the Calla solution.

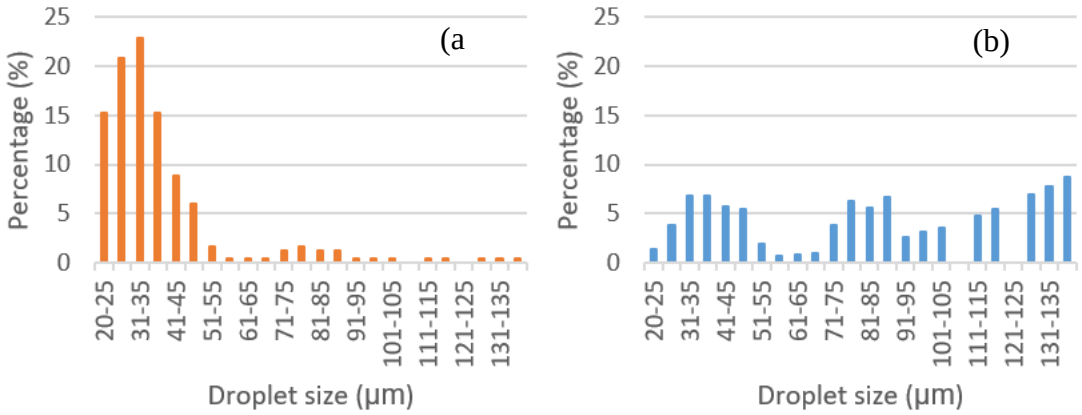

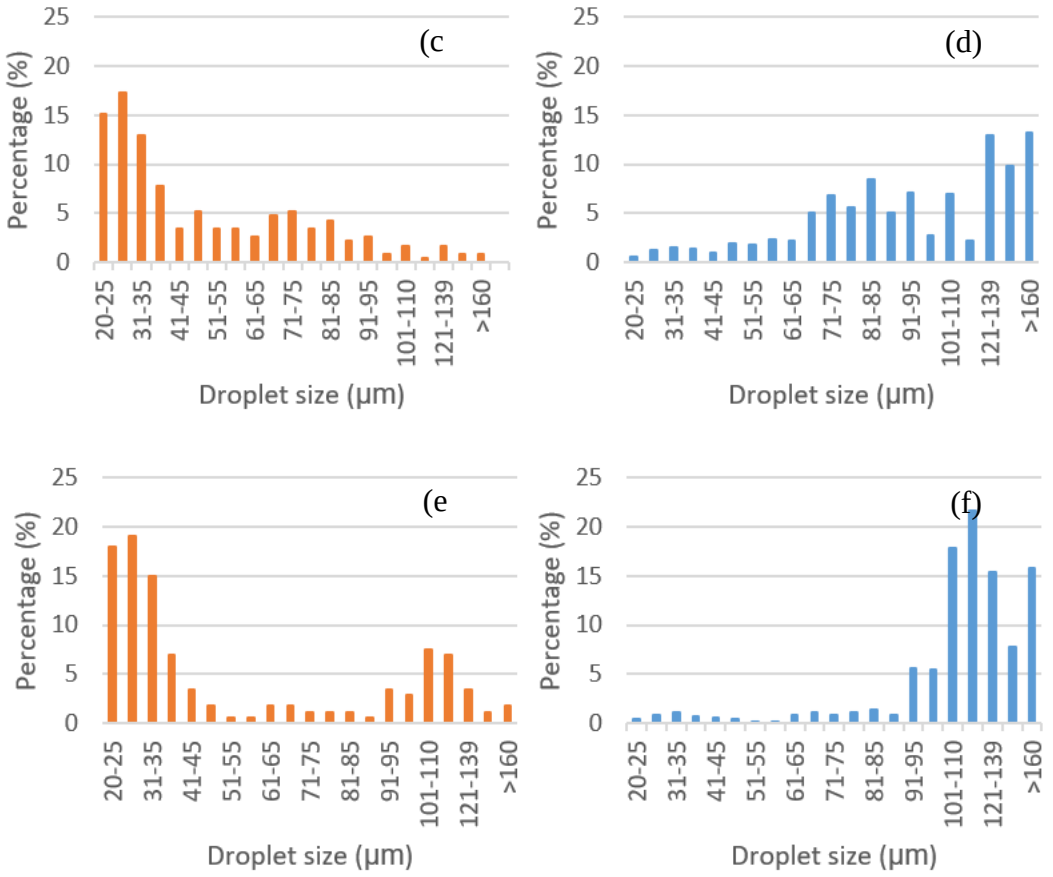

Figure 2. Droplet size distribution measured by the GSV system for the Protexus sprayer with the Calla 1452 solution. (a) 40-µm nozzle setting; number distribution, (b) 40-µm nozzle setting; volume distribution, (c) 80-µm nozzle setting; number distribution, (d) 80-µm nozzle setting; volume distribution, (e) 110-µm nozzle setting; number distribution, (f) 110-µm nozzle setting; volume distribution.

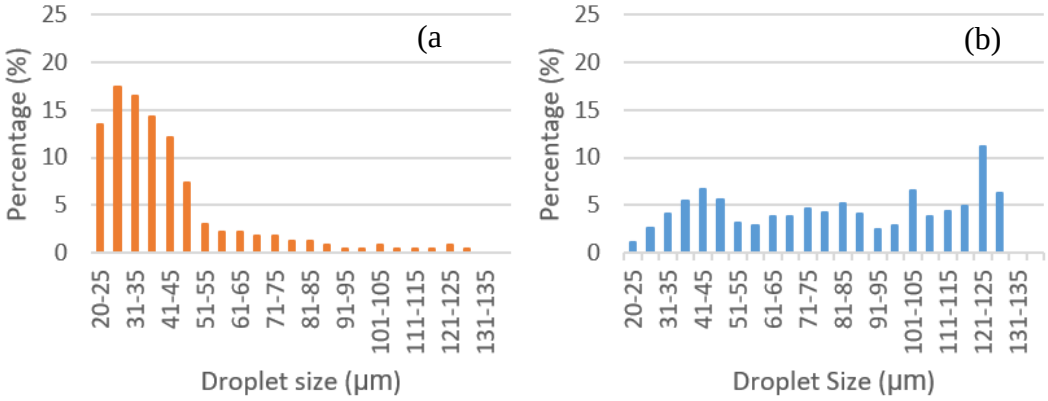

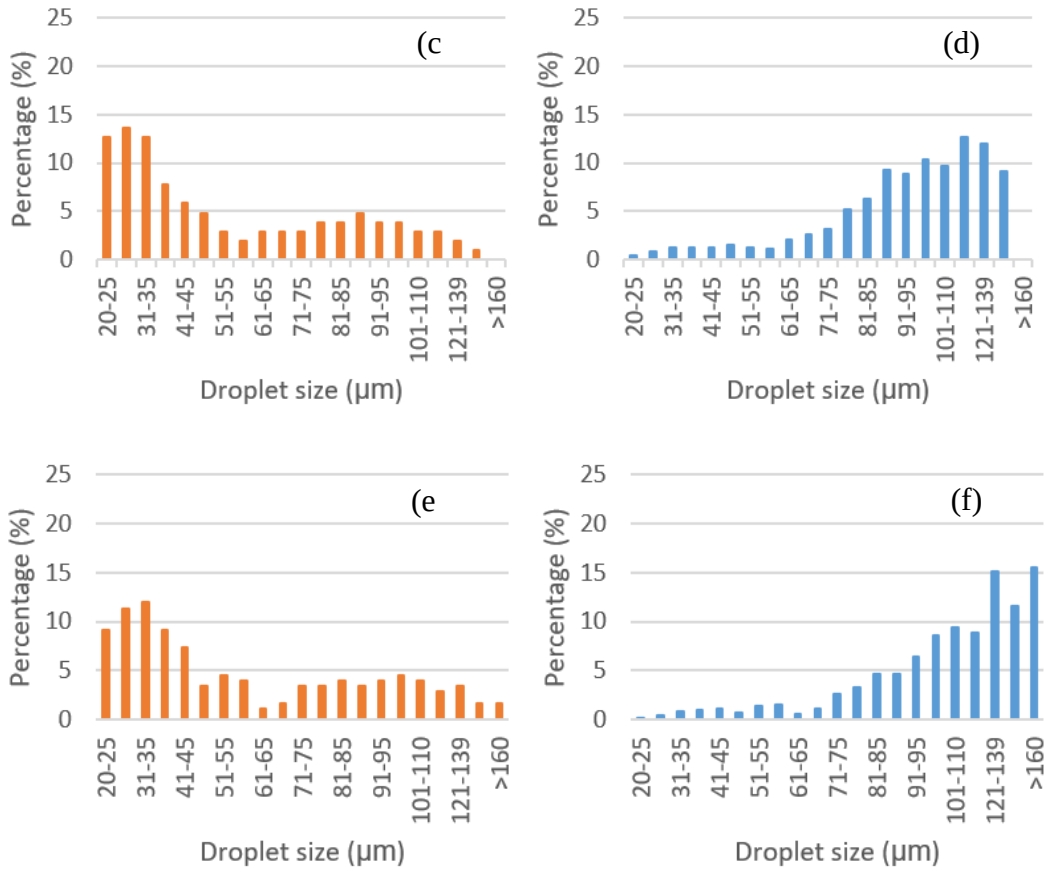

Figure 3. Droplet size distribution measured by the GSV system for the Protexus sprayer with the Peroxi solution. (a) 40-µm nozzle setting; number distribution, (b) 40-µm nozzle setting; volume distribution, (c) 80-µm nozzle setting; number distribution, (d) 80-µm nozzle setting; volume distribution, (e) 110-µm nozzle setting; number distribution, (f) 110-µm nozzle setting; volume distribution.

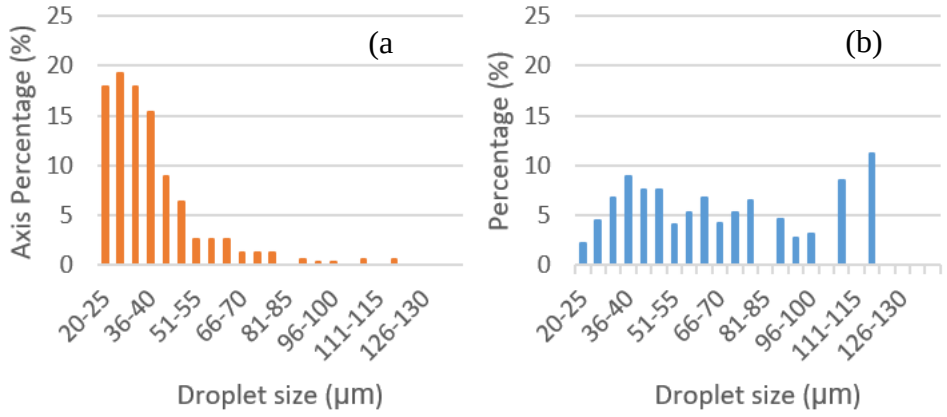

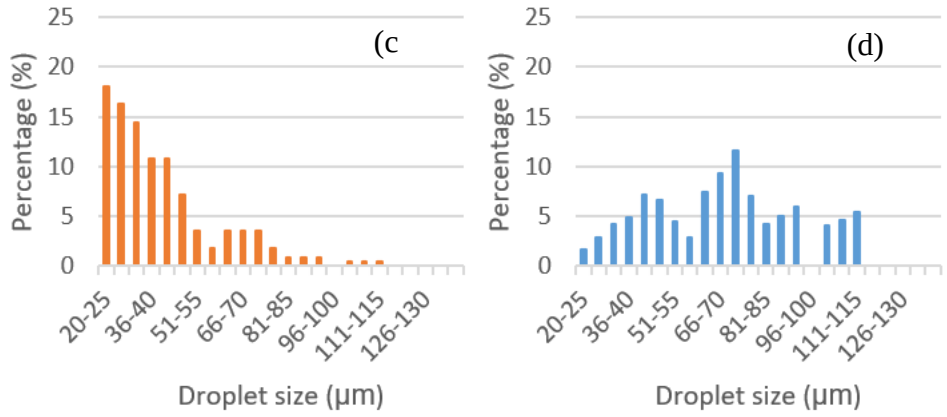

Figure 4. Droplet size distribution measured by the GSV system for the SC-EB sprayer. (a) Calla solution; number distribution, (b) Calla solution; volume distribution, (c) Peroxi solution; number distribution, (d) Peroxi solution; volume distribution.

Table 1. Mean droplet size (NMD and VMD) measured by the GSV method.

Droplet Charge Measurement

1. Deflection velocity method

As mentioned previously, two parallel plates with an electric field intensity of 1 kV/cm (8 kV, 8 cm) were installed at our measurement area, which deflected the charged droplets in between. The GSV system was applied to track the deflection velocity in the horizontal direction for each detected droplet. Figures 5(a) and (b) give an example of the velocity vectors of the droplets from the Protexus sprayer inside the parallel plates, which were measured by the GSV system. The two bars in blue in each figure represents the parallel plates. The left plate is grounded while the right plate is positively charges. With the droplets drifting towards left, it can be identified that the droplets generated by the Protexus sprayer were positively charged. The vectors were colored by the velocity magnitude of the droplets.

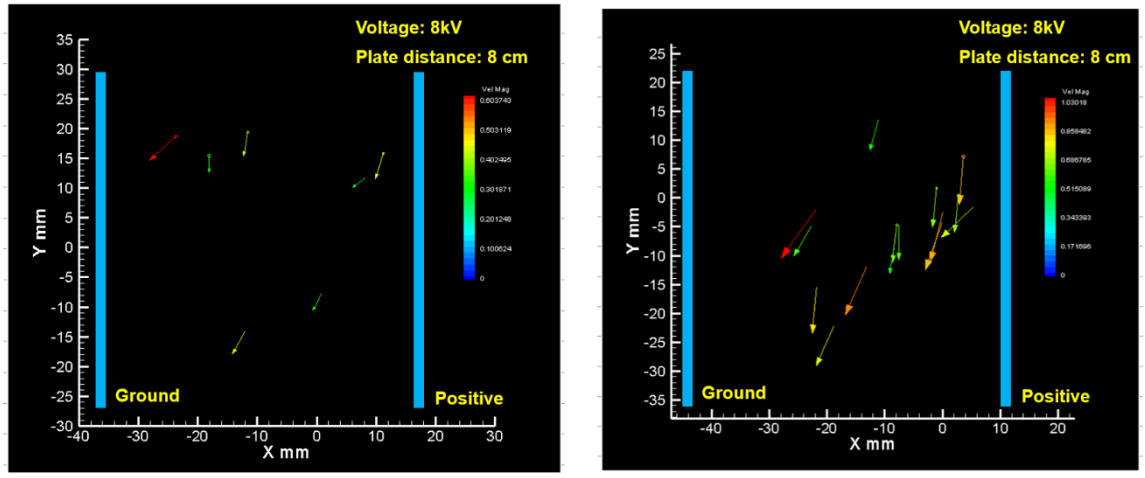

Figure 5. Velocity vectors colored by the velocity magnitude measured by the GSV system for the charged droplets between two parallel plates. The droplets were generated by the Protexus sprayer with (a) the 40-μm nozzle and (b) 110-μm nozzle.

The droplet charge is obtained by equating the electrostatic force to Stokes drag and solving for charge, n, which is given in the following equations.

$$neE = 3\pi\eta Vd\ , \tag{1}$$

$$n = \frac{3\pi\eta Vd}{eE}\ , \tag{2}$$

where e is the elementary charge and equal to 1.602×10^{-19} C, E is the electric field intensity and equal to the voltage difference divided by the distance between the parallel plates, η is the air dynamic viscosity and equal to 1.846×10^{-5} kg/(m-s), V is the droplet deflection velocity and d is the droplet diameter. Both V and d were measured by the GSV systems for each detected droplet. The calculated mean droplet charges of all cases are summarized in Table 2. The results indicate that droplets from the Protexus spray and SC-EB spray are positively and negatively charged, respectively. And the SC-EB spray has higher charge levels for both solutions in general.

Table 2. Mean droplet charge measured by the deflection velocity method.

	Protexus Spray			SC-EB Spray
	40-μm Nozzle	**80-μm Nozzle**	**110-μm Nozzle**	
Calla Solution	1.02×10^5	1.78×10^5	1.21×10^5	-6.34×10^5
Peroxiguard Solution	8.72×10^4	1.31×10^5	1.06×10^5	-4.53×10^5

2. Direct electric charge measurement by an electrometer

Another droplet charge level measurement was conducted to measure the average charge level of the entire plume of droplets generated from the sprayers. This method is based on a direct electric charge measurement using an electrometer, as a schematic shown in Figure . Since the induction charging ring inside the sprayer head generates a non-negligible level of electric field in surrounding space, a home-made Faraday cage is used to isolate the impact of this electric field to the current measurement. The Faraday cage is made of high conductive brass with 3/8" thick wall and an opening just big enough to allow all droplets from the sprayer to enter. To further minimize the effect from any external electric field, the Faraday cage is located inside a stainless steel shielding can, supported by a large piece of Teflon block to avoid any electric current exchange (by contact) between the shielding can and the Faraday cage. This configuration allows the Faraday cage to collect charges carrying by those droplets from the sprayer which is simultaneously measured as electric current by a self-grounded electrometer (Keithley 6517B), but successfully suppress the interference current level that is induced by the sprayer head itself (not from the charges carrying by droplets). As shown in Table , the current measured during normal spraying operation is between 0.01 and 10 μA depending on sprayer and nozzle selection, while the interference current by the sprayer head when the spraying is not triggered (air flow is on for SC-EB sprayer) is well below 0.1 nA, yielding a signal-to-noise ratio of 100 or higher. Such interference current would be significantly higher if the shielding was not used (~20 nA) or the sprayer head was inserted into the envelope of the Faraday cage (~50 nA for Protexus sprayer and ~1 μA for SC-EB sprayer). It was also found interestingly that the SC-EB sprayer could not generate any current signal (droplet charge or interference current) if the 9V battery in the sprayer was removed, suggesting that low-voltage battery is powering up the droplet charging mechanism inside the sprayer head.

The current measured by electrometer in this method represents the total amount of electric charges carrying by the droplets from the sprayer per unit time. In order to convert it into the mean charge per droplet, the droplet generation throughput (how many droplets generated per unit time) is determined based on mass conservation and the volume mean diameter from GSV measurement. The liquid volume throughput is measured by directly spraying liquid into a measuring tube (a 100-mL unit for Protexus sprayer and a 1000-mL unit for SC-EB sprayer) and calculated by dividing the liquid volume collected by the spraying time. Since the average volume of each individual droplet can be calculated using the volume mean diameter, the average number of droplets generated per unit time is determined, as shown in Table 3.

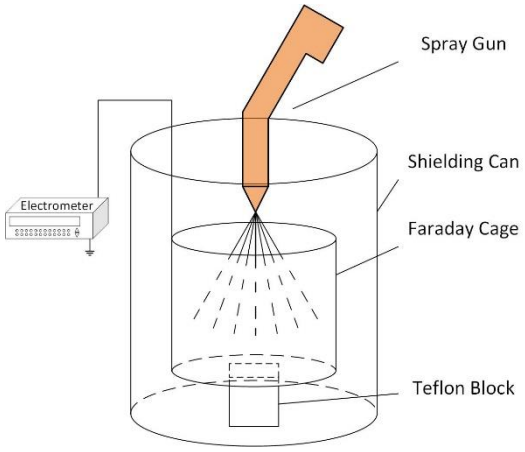

Figure 6. Schematic of mean droplet charge measurement using Faraday-cage and electrometer.

Table 3. Data summary of mean charge measurement using Faraday-cage and electrometer.

	Protexus Sprayer						SC-EB Sprayer	
	40-µm nozzle		80-µm nozzle		110-µm nozzle			
	Calla	Peroxigard	Calla	Peroxigard	Calla	Peroxigard	Calla	Peroxigard
Liquid collection Time (s)	23.1		18		6.2		120	
Liquid collected (mL)	41		42		36		190	
Liquid throughput (m^3/s)	1.77×10^{-6}		2.33×10^{-6}		5.81×10^{-6}		1.58×10^{-6}	
Volume mean droplet diameter (µm)	84.5	81.5	103.3	99.0	118.2	114.1	67.8	68.8
Droplet # throughput (#/s)	5.62×10^6	6.26×10^6	4.04×10^6	4.59×10^6	6.72×10^6	7.47×10^6	9.70×10^6	9.29×10^6
Current measured by electrometer (µA)	0.02	0.015	0.075	0.057	0.11	0.08	-5.5	-8.3
Mean coulombic	2.22×10^4	1.50×10^4	1.16×10^5	7.76×10^4	1.02×10^5	6.70×10^4	-3.54×10^6	-5.59×10^6

charge per droplet								

Droplet Size Calculation Based on the Measured Settling Velocity

The GSV system was also utilized to measure the settling velocity of the droplets generated by the Protexus sprayer with the two solutions. The measurements were conducted without the two parallel plates to eliminate the effect of the electric field on the droplet movements. The terminal settling velocity of each droplet is given by

$$V_{TS} = \frac{\rho_d D_d{}^2 g}{18\eta_a}, \tag{3}$$

where ρ_d is the droplet density which is estimated to be 997 kg/m^3, η_a is the dynamic viscosity of air, 1.846 × 10^{-5} kg/(m-s), and D_d is the droplet diameter related to the terminal settling velocity. Once the settling velocity is measured, the droplet diameter is calculated as

$$D_d = \sqrt{\frac{18\eta_a V_{TS}}{\rho_d g}}\,. \tag{4}$$

To compare the droplet size calculated based on the settling velocity, D_d, with the droplet size measured by the GSV system, d, we defined a ratio, r, as

$$r = \frac{D_d}{d}. \tag{5}$$

Figures 7(a) and (b) show the ratio, r, at different measured droplet size. For droplet size larger than 80 μm, r is close to 1, indicating there is good agreement between the caclualted droplet size and the measured droplet size. At smaller droplet size, the settling velocity method overestimates the droplet size due to the fact that the measuerment on smaller droplets' settling speeds can be easily affected by the disturbance and turbulence in the airflow.

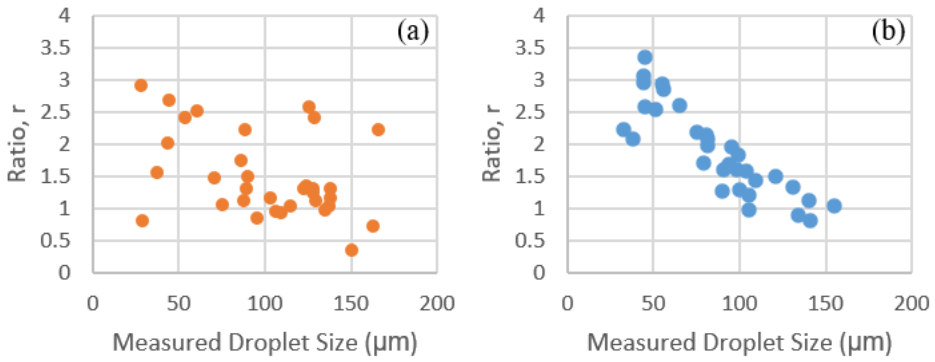

Figure 7. Ratio, *r*, as a function of measured droplet size for the Protexus sprayer with (a) the Calla 1452 solution and (b) the Peroxigard solution.

Conclusions

The evaluation of the EvaClean ™ Protexus and ESS SC-EB sprayers has been completed, and the droplet number throughputs, size distributions and mean droplet electrostatic charges were obtained for all spray system and disinfectant combinations. Our main method is the GSV system, which measures the droplet size by analyzing the light scattering oscillation patterns and calculates the droplet mean charge by measuring the deflection velocity between two parallel plates with high voltage. The Faraday cage and electrometer system is a new setup in our lab, and it was intended to validate the mean charge results from GSV. There is some discrepancy on the charge values between the electrometer and GSV methods, but it demonstrates that the results from the GSV system is reasonable. Therefore, we summarized our measurement results on the liquid throughput, droplet number throughput, droplet mean diameter and mean charge per droplet in the following Table 4.

Table 4. Summary of the measurement results for the evaluation of the Protexus and SC-EB sprayers.

	Protexus Sprayer												SC-EB Sprayer			
	40-μm nozzle				80-μm nozzle				110-μm nozzle							
	Calla		Peroxigard		Calla		Peroxigard		Calla		Peroxigard		Calla		Peroxigard	
Liquid throughput (m^3/s)	1.77×10^{-6}				2.33×10^{-6}				5.81×10^{-6}				1.58×10^{-6}			
Droplet # throughput (#/s)	5.62×10^{6}				6.26×10^{6}				4.04×10^{6}				4.59×10^{6}			
Droplet Mean Diameter (μm)	NMD	VMD	NMD	VMD	NMD	VMD	NMD	VMD	NMD	VMD	NMD	VMD	NMD	VMD	NMD	VMD
	42.0	84.5	43.2	81.5	51.6	103.3	55.7	99.0	54.3	118.2	59.1	114.1	37.9	67.8	41.7	68.8
Mean coulombic charge per droplet	1.02×10^{5}		8.72×10^{4}		1.78×10^{5}		1.31×10^{5}		1.21×10^{5}		1.06×10^{5}		-6.34×10^{5}		-4.53×10^{5}	

8.4 ES Device Characterization: Boeing Research per ASTM D7952

Research was conducted at Boeing to determine spray pattern as defined in ASTM D7952. This was used for ES nozzle size selection on the Protexus sprayer, since multiple size nozzles were available.

A 6.0 cm aluminum cup was weighed on a balance accurate to 0.0001 g. The sprayer nozzle and cup were positioned in the configuration shown in Figure 4.

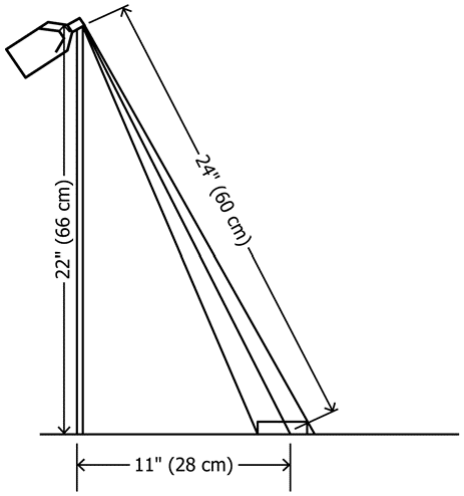

Figure 4: Orientation of Sprayer to Test Cup per ASTM D7952

The inside of the cup was sprayed for 5 to 7 seconds, while time was recorded with a stopwatch accurate to 1/100th seconds. The cup was re-weighed with the deposited spray within 60 seconds, and the measurement was repeated 3 times. The testing was done at an ambient temperature of 20 ± 2°C in a draft free room.

As shown in Table 2, a large amount of variance in the data is apparent from the wide 95% Confidence Intervals (CI). The large variance was due to a small sample size, overspray of the cup, spray velocities and sampling bias. However, ASTM D7952 did facilitate the characterization of the droplet distribution shape by ES devices and disinfectants.

As defined in ASTM D7952, a cone shaped spray has an average deposition rate of between 0.05 g/s but less than 0.75 g/s. Deposition rates less than 0.05 g/s are classified as mists and deposition rates greater than 0.75 g/s are classified as streams. In addition, ASTM D7952 defines a cone shaped spray as completely covering the bottom of the test cup but also extending beyond the edge of the test cup. In all cases, the droplet distribution shape was found to be a cone shaped spray. The cone shaped spray is considered ideal since it provides sufficient coverage, unlike the mist, without making the surface “too wet”, like the stream. This evaluation was not intended to compare deposition rates between sprayers.

Table 2: ES Model Deposition Rate per Second

ES Model	Chemical	Mean (g/s)	Standard Deviation (g/s)	95% CI (g/s)
Emist	Peroxi™ RTU	0.13	0.016	±0.040
Protexus (40µ)	Peroxi™ RTU	0.083	0.022	±0.055
Protexus (80µ)	Peroxi™ RTU	0.07	0.01	±0.025

ESS	Peroxigard™ RTU	0.123	0.015	±0.037
Emist	Calla®	0.073	0.011	±0.027
Protexus (40µ)	Calla®	0.087	0.038	±0.094
Protexus (80µ)	Calla®	0.215	0.026	±0.065
ESS	Calla®	0.162	0.028	±0.070

8.5 Expanded DOE 1 Methodology

The data collection for the DOE 1 study was done in phases with an initial DOE, called Bridge 0 DOE, and then additional DOEs, called Bridge 1 to 3 DOEs. The goal of the bridge DOEs was to systematically build bridges between the existing test conditions and new test conditions so that all of the data could be combined into a final statistical model that related inputs to outputs and also to quantify which inputs had a larger effect on the outputs.

After each Bridge DOE, conditions were added to leverage the results from the previous bridge. The following Tables 8 to 11 outline the process variables studied in each bridge.

Table 8: Variable Input Parameters for Bridge 0 of DOE1.

Bridge 0 DOE	
Sprayer	ESS SC-MB Sprayer; EMist EM360 (85 µm) Sprayer
Disinfectant	Peroxi™ RTU; Calla®
Surface	Porous; Non-porous
Spray Time	5 seconds; 10 seconds
Spray Distance	2 feet; 4 feet; 6 feet
Fan Circulation	Circulation; No Circulation
Orientation	Sample on ground: sprayed perpendicular, and down at 45°; Sample on wall: sprayed perpendicular, up and down at 45°
Replications	2x per condition

A significant change in Bridge 1 was the addition of data collection on the Protexus sprayer.

Table 9: Variable Input Parameters of the Bridge 1 of DOE1.

Bridge 1 DOE	
Sprayer	EvaClean™ Protexus Sprayer (40 and 80 µm)
Disinfectant	Peroxi™ RTU; Calla®
Surface	Non-porous
Spray Time	5 seconds; 10 seconds
Spray Distance	2 feet; 4 feet; 6 feet
Fan Circulation	Circulation; No Circulation
Orientation	Sample on ground: sprayed perpendicular, and down at 45°; Sample on wall: sprayed perpendicular, up and down at 45°
Replications	2x per condition

Table 10: Variable Input Parameters of the Bridge 2 of DOE1.

Bridge 2 DOE	
Sprayer	EvaClean™ Protexus Sprayer (40 and 80 µm); SC-MB Sprayer; EMist EM360 (85 µm) Sprayer
Disinfectant	PREempt™; Matrix #3
Surface	Non-porous
Spray Time	5 seconds;10 seconds
Spray Distance	2 feet; 4 feet; 6 feet
Fan Circulation	No Circulation
Orientation	Sample on ground: sprayed perpendicular; Sample on wall: sprayed perpendicular; Sample at 45°: sprayed perpendicular, up and down at 45°
Replications	2x per condition

Orientation (on wall or on ground) was determined to be a significant factor. Because of this, only data on angled surfaces was taken in the following DOE bridge.

Table 11: Variable Input Parameters of the Bridge 3 of DOE1.

Bridge 3 DOE	
Sprayer	EvaClean™ Protexus Sprayer (40 and 80 µm); SC-MB Sprayer; EMist EM360 (85 µm) Sprayer
Disinfectant	Peroxi™ RTU; Calla®
Surface	Porous, Non porous
Spray Time	5 seconds, 10 seconds
Spray Distance	2 feet, 4 feet, 6 feet
Fan Circulation	No Circulation
Orientation	Sample at 45°; sprayed perpendicular, up and down at 45°
Replications	1x per condition

8.6 Expanded DOE 2 Methodology

The goal of the IR video analysis was to quantify spray coverage and dry time of a material sample when sprayed with an ES device. It was desirable that the process for generating these estimates was as automated as possible in order to enhance reproducibility and reduce subjective bias. Therefore, an analysis pipeline was developed which included minimal manual steps and could calculate spray coverage and dry-times from IR videos directly.

Figure 22 gives an overview of the analysis methods used in DOE2.

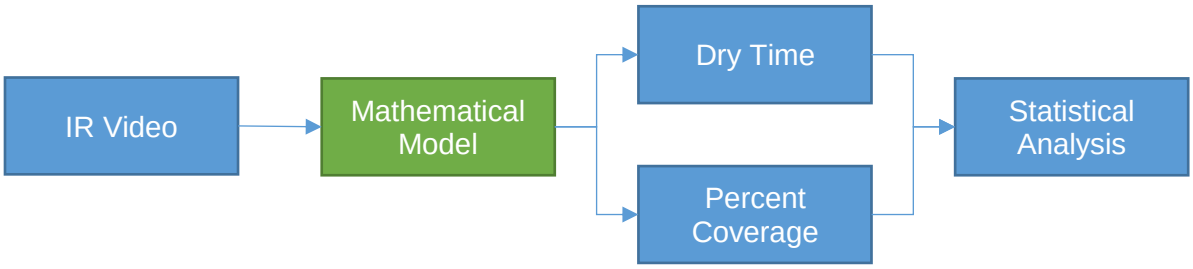

Figure 22: Analysis methods in DOE 2.

The pipeline had two manual steps:

1. Determining the time when the experimenter finishes spraying, called spray-time.
2. Drawing a polygon around the ROI.

All drying times were calculated relative to the spray-time for a given video. The second step, drawing a polygon around the ROI, was used to exclude irrelevant pixels from analysis.

Due to several unexpected sources of noise, the analysis pipeline could not be accurately applied to all videos. In these cases, manual estimates were used or the videos were excluded from further analysis. The team is confident that the analysis method represents a reliable and promising method for characterizing material drying properties.

Spray-time and region of interest selection

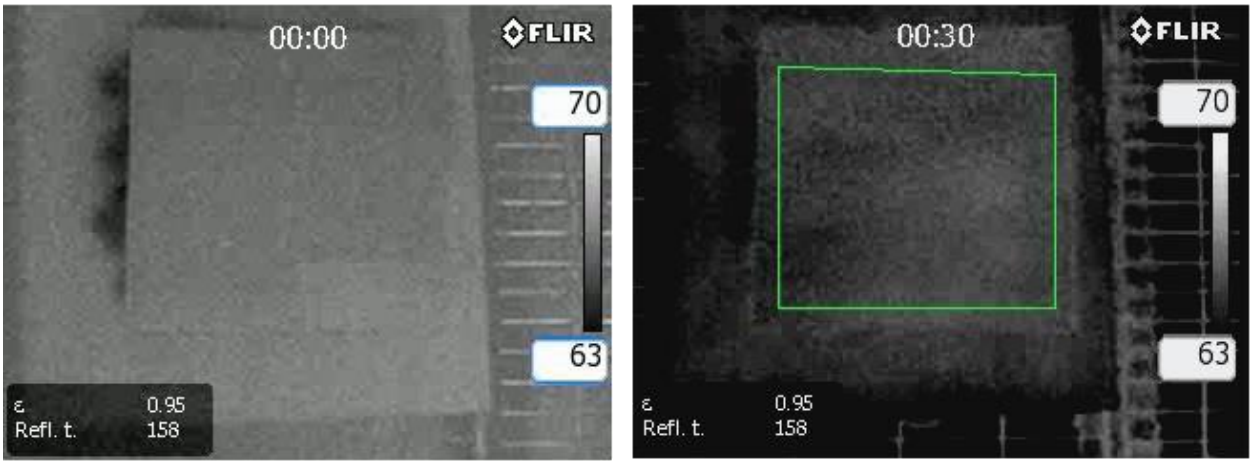

a b

Figure 24: IR video frames before (Left) and after spray (Right) with region of interest shown in green

Effect of electrostatic spray on grayscale pixel intensity values

Once loaded, each frame initially contained three color channels and was first converted to a grayscale image. The grayscale image was a 240 x 320 matrix of 8-bit unsigned integers each taking on values from 0 – 255. These intensity values were representative of temperature in the sense that warmer regions of the frame resulted in larger pixel values and cooler regions resulted in smaller pixel values, however it was not possible to extract calibrated temperature values for each pixel. For the purposes of this experiment, only having pixel intensities was sufficient.

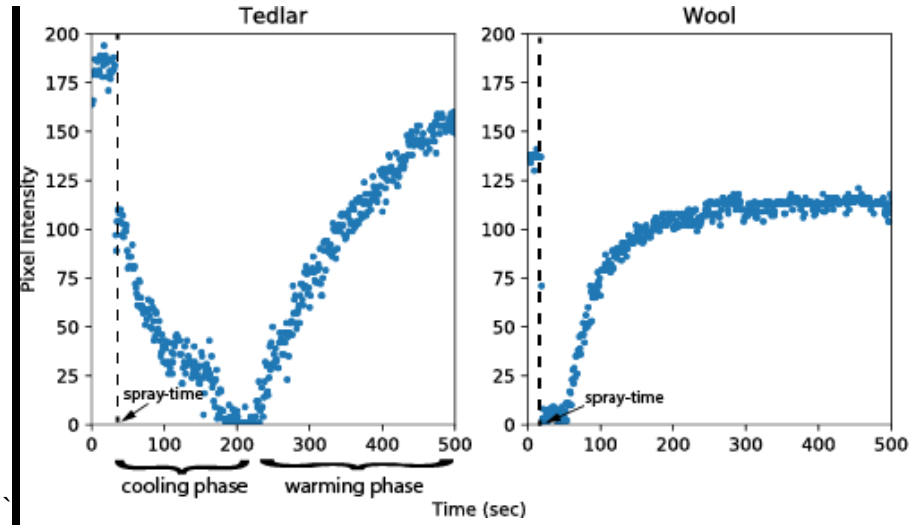

Figure 25: Different materials exhibit different pixel intensity profiles after being sprayed

Pixel intensities as a function of time exhibit a common pattern after being sprayed. Typical pixel intensity profiles for two different materials are shown in **Error! Reference source not found.**. At the time of spray, there is a rapid drop in pixel intensity, followed by a more gradual drop and rise in intensity during what is referred to as the cooling and warming phases. These phases are clearly shown in the Tedlar material of **Error! Reference source not found.**. The cooling phase is presumably caused when the thin film deposited by the electrostatic sprayer is evaporating from the surface of the target object. During the warming phase the pixel intensity quickly ramps up and eventually levels off as that portion of the target object reaches thermal equilibrium. The duration of these phases can vary depending on the thickness of the deposited film, the material properties of the target object, and the environmental conditions such as temperature and humidity. For example, the wool material of **Error! Reference source not found.** has almost no cooling phase.

Quantification of electrostatic spray coverage

In order to characterize the spray coverage over a target object, a binary value was assigned to each pixel to indicate whether the portion of the target object represented by that pixel received a measurable amount of spray. Specifically, the test evaluated whether or not there was a significant drop in pixel intensity between a four second duration at the start of the video and a one second duration after the identified spray-time for that video.

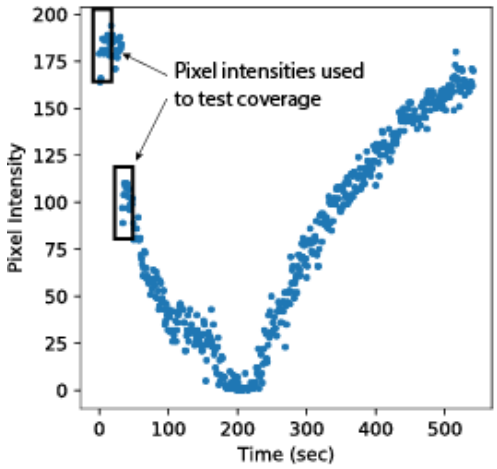

Figure 26: Example pixel showing intensities used to test coverage

For each pixel in the video's ROI, we calculated p-values using a two-sample t-test and corrected for multiple tests to have a false discovery rate of 0.05. Spray coverage was reported as the percentage of pixels within a ROI that had a significant change.

Quantification of dry-times

In order to quantify the dry-time, a mathematical model was developed and fit to the raw IR pixel data. This model allowed for more accurate processing than working with the raw data directly.

The developed model for temperature is given by the map $\hat{u}(t; a_{1:3}, b_{1:3}, \gamma): R^8 \to R$ having the form:

$$\hat{u}(t; a_{1:3}, b_{1:3}, \gamma) = \begin{cases} a_1 + a_2 t + a_3\sqrt{t}, & t \le \gamma \\ b_1 - \exp(b_2 t + b_3), & t > \gamma \end{cases}$$

Where t is time, $a_{1:3}$ are the model coefficients for the evaporative cooling phase, $b_{1:3}$ are the model coefficients for the warming phase, and γ is the breakpoint time where the model switches from cooling to warming. The parameters a_2, a_3, and b_2 are constrained to be less than zero. This model makes several simplifying assumptions. The evaporative cooling phase assumes the target object is a sufficiently thick semi-infinite body,[9], and the warming phase assumes conductive heat transfer with no spatial variation and an energy rate density proportional to the difference between the target object and the temperature of the room. To get the final functional form of our model, the breakpoint is directly estimated by adding the constraint.

$$\begin{aligned} a_1 + a_2\,\gamma + a_3\sqrt{\gamma} &= b_1 - \exp(b_2\,\gamma + b_3\,) \\ a_1 + a_2\,\gamma + a_3\sqrt{\gamma} + \exp(b_2\,\gamma + b_3\,) &= b_1 \end{aligned}$$

The piecewise function $\hat{u}$ is implemented using max so that

$$\hat{u}(t; a_{1:3}, b_{2:3}, \gamma) = \max \begin{cases} a_1 + a_2 t + a_3 \sqrt{t}, \\ a_1 + a_2\, \gamma + a_3 \sqrt{\gamma} + \exp(b_2\, \gamma + b_3\,) - \exp(b_2 t + b_3). \end{cases}$$

This functional form is fit to each individual pixel using non-linear least squares. An example model fit is shown by the red curve in **Error! Reference source not found.**.

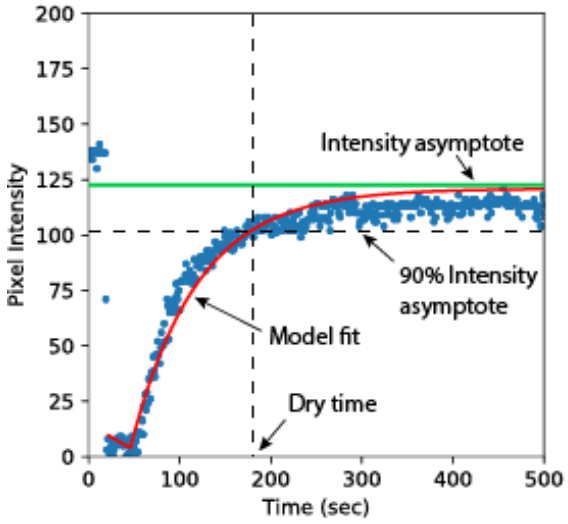

Figure 27: Example pixel showing how dry-time was determined from the model

In this figure, the value for the asymptote of the warming phase is shown by the green line, which is used to determine the dry-time by finding the point where the model curve crosses a threshold set at 90% of the warming asymptote. Setting the threshold to 90% of the warming asymptote is a heuristic, which is rationalized since it is where the pixel intensity is “close enough” to thermal equilibrium, and well past the point governed by evaporative cooling. The reported dry-time for a ROI is the 90th percentile of the dry-times for all pixels in the ROI.

8.7 Future Work in Boeing Research & Technology

This paper presented initial research findings and recommendations on semi-automated disinfection methods. These methods provide the ability to disinfect surfaces more consistently and efficiently than manual application of chemicals. The two studies presented, DOE 1 and DOE 2, characterized the electrostatic sprayer operational parameters and provided understanding of how environmental variables change electrostatic spray effectiveness.

Since regular disinfecting of all interior surfaces of the aircraft is an objective to address the emergent health concerns related to COVID-19, additional studies are necessary to further understand the impact of these new processes and disinfectants. Boeing has several in-depth studies that are ongoing and seek to assess:

1. The potential of surface degradation (i.e. corrosion, surface fouling) from spraying.
2. The potential of functional degradation (in critical and non-critical aircraft parts) from spraying.
3. The efficacy of the disinfecting process using an ES device in a cabin mockups using live surrogate and SARS-COV2 virus.

The following summarizes the ongoing research studies and their expected outcomes:

1. **DOE 3: Repeat Application for Material Compatibility** examines resulting surface degradation (i.e. corrosion, surface fouling) from spraying.
2. **DOE 4: Functional Degradation of Electrical Components** assesses functional degradation (in non-critical aircraft parts) from spraying.
3. **Chemical Disinfection Investigations for Flight Deck Equipment** assesses functional degradation (in critical aircraft parts) from spraying.
4. **DOE 5: Computational Fluid Dynamics** develops models that enable rapid assessment of new disinfectants and sprayers.
5. **DOE 6: Evaluation of Aircraft Seats** assesses the surface impacts of spraying on seats.
6. **Live-Virus Testing** evaluates the efficacy of electrostatic spray application and its ability to provide effective disinfection.

The findings of these studies are expected to be used to develop additional recommendations and guidance to our airline partners on spray application methods and substrate impacts. Boeing anticipates release of the results of DOE3, DOE4, and DOE5 by the end of November 2020.

DOE 3: Repeat Application for Material Compatibility

Long-term material compatibility between aircraft interior materials and repeated application of disinfectant was evaluated. DOE 3 is designed to simulate the repeated use of disinfectant and potential accumulation of residue that an aircraft would see over its lifetime if disinfected regularly.

Surface testing on an array of representative coupons is being conducted. Two replicate sets of materials, were sprayed by a quaternary ammonium chloride (QAC) solution, and accelerated hydrogen peroxide (AHP) solution. 249 coupons have been evaluated between both disinfectant solutions, covering an array of material categories representing different components in the passenger cabin. Each sprayer was set to a nominal condition, and allowed for a full and complete dry time (30 minutes), before re-application. Substrates were imaged at intervals for evaluation of corrosion, discoloration, and other signs of degradation over time. Each sample was sprayed to a total of 400 cycles, representative of slightly over one year of operation sprayed 1 time per day.

Coupons sprayed with the disinfectants were evaluated for signs of corrosion on the metals, signs of physical damage (e.g., crazing, blistering) and discoloration on the thermoplastics, and breaking strength and also discoloration on the fabrics. Below are the findings from the evaluation:

1. Exposure to the two disinfectants did not appear to degrade hard non-porous cabin interior materials such as polycarbonate, PVF/PEKK, Ultem, and Tedlar upon visual inspection. The same observations were made on stainless steel, deionized water-sealed anodized aluminum, and BMS10-121 coating.
2. BMS10-11 and BMS10-83 coatings had adhesion failures with the AHP disinfectant but not with the QAC.

DOE 4: Evaluation of Electrical Components

Long-term functional degradation was assessed on a set of 33 airplane line replaceable units

(LRUs). DOE 4 was designed for repeat application of Calla, to simulate the long term performance impact of regular disinfection on the airplane.

High-touch parts from the cargo, cabin, lavatory and in-flight entertainment sections of the aircraft were autonomously sprayed with Calla 1000 times. At set intervals, the components were evaluated for functional degradation by a unique performance standard. These tests ranged from simple resistance measurements, to fully integrated testing in Boeing's Cabin Systems and Avionics Integration Labs. The study found that 1000 spray cycles of Calla did not impact the functional performance of the components.

Chemical Disinfection Investigation: Flight Deck Equipment

Long-term functional degradation was assessed on critical aircraft parts in the flight deck. Studies were conducted in the 777 engineering cab, and on isolated components in the Boeing Development Center. 11 pieces of equipment were selected by Flight Deck Engineering from the 737 and 787 models as representative of most BCA airplane equipment, and these 11 articles were sprayed at nominal conditions using nozzle distance and rates of traverse derived from observation of trained personnel spraying 737 and 777 flight decks.

Peroxigard was discontinued due to apparent etching of a conformal coating after 20 applications and at a time coincident with the first negative coupon results from the BDC robot testing. Calla was discontinued after 210 applications based on observations made during visual and functional assessments performed after 130 applications, consisting of rust development on a component where residue began to accumulate, and after 210 applications, consisting of functional failures of several pieces of equipment and corrosion of electronics on printed wiring boards. The hardware testing in DOE 4 was not flight-critical, so Calla 1452 application was continued in this study. Further evaluation of safety-critical flight hardware is necessary prior to recommending the technology for general use.

DOE 5: Computational Fluid Dynamics

A theoretical computational fluid dynamics (CFD) model is being developed to simulate spray application, wetting, film thickness, and drying. DOE 5 is designed to validate CFD model to demonstrate how sprayers interact with an actual cabin. The model, once verified, could be used to assess new disinfectants, sprayers, or hardware in a shorter time than physical testing.

A 6-row, cross section of a retired 737 NG was used to generate representative cabin airflow. A mockup evaluation was run to cross reference the virtual and physical test environments. An ES device was introduced into the CFD model in order to virtually deposit disinfectant onto hardware within the cabin. Once the physical mockup and sprayer match the CFD model, regions of interest will be identified and evaluated via spray application within the mockup, thermal IR video capture, and pixel density contrast change analysis. The data collected from DOE 1 and DOE 2 became inputs for DOE 5 and is being used to evaluate and train the CFD model completely.

DOE 6: Evaluation of Aircraft Seats

Aircraft disinfection most commonly takes place during the aircraft's turnaround time, meaning the flying public will soon be boarding the aircraft and taking a seat. In order to minimalize dissatisfaction of the flying public, it is important to ensure that when seating is taking place, all the seats have dried completely to avoid saturating a passenger's clothing. DOE 6 examined 10

different seat configurations to study their drying characteristics with two spray disinfectants and studied under different environmental conditions: ambient or elevated temperature with ambient or elevated humidity. The study included economy class seats, business class seats, leather seats, and cloth seats.

A test matrix was developed for testing in the Boeing 2-10 building where a thermal IR camera and analysis was employed to determine the dry time of each seat. The testing space contained temperature and humidity control through the use of a heater and steamer, in combination with a fan to pump air into the test area. The primary areas of interest of the study were the seat cushion, the back rest, the head rest, and the arm rest areas – areas that a passenger immediately contacts upon taking a seat. Based on the analysis of the collected data, the outcome of this DOE indicated that the dry time depended on temperature and humidity conditions, which may have been impacted by airflow that was turned on or off to simulate the environmental conditions. With airflow on, the drying times for both disinfectant were similar and seats were completely dry within a handful of minutes or less. These conditions are favorable to meet the turnaround time for many airlines.

Live-Virus Testing

To understand the efficacy of electrostatic spray application and its ability to provide effective disinfection, Boeing contracted with live virus labs to test cabin mockups at test facilities using both surrogate and SARS-CoV-2 virus.

First, a working airflow cabin mockup was sent to a Biosafety Level 2 facility in order to test the ability of the ES device disinfection process to kill a surrogate virus.

Using this data, a correlation study will be developed to mathematically associate the surrogate virus kill efficiency to that of SARS-CoV-2. A separate study will utilize a non-airflow cabin mockup in a Biosafety Level 3 facility to test against SARS-CoV-2 samples. The testing of the surrogate virus and SARS-CoV-2 virus will continue until the end of 2020 with anticipated results to be shared by early 2021.

Frasers Aerospace - Internal Notes:
Bacoban for Aerospace only available from Frasers Aerospace
Bacoban for Aerospace 1% DL Hand Spray Application Bottle - https://www.frasersaerospace.com/product/bacoban-for-aerospace-disinfectant/
Bacoban for Aerospace 1% DL Pack of Wipes - https://www.frasersaerospace.com/product/bacoban-for-aerospace-wipes/
Bacoban for Aerospace 3% DL Fogging / Nebuliser type - https://www.frasersaerospace.com/product/bacoban-for-aerospace-3-fogging-type/